Observation of orbital moment in NiO

V. Fernandez and C. Vettier
European Synchrotron Radiation Facility, Boîte Postale 220 38043, Grenoble Cedex, France

F. de Bergevin
Lab. Cristallographie CNRS, Boîte Postale 166 30842, Grenoble Cedex, France

C. Giles
Universidade Estadual de Campinas, C.P. 6165, 13083-970 Campinas, Brazil

W. Neubeck
European Synchrotron Radiation Facility, Boîte Postale 220 38043, Grenoble Cedex, France
(Received 31 October 1997)

The spin- and orbital-moment magnetization form factors in NiO have been measured using magnetic x-ray scattering. The polarization analysis of nonresonant magnetic-scattering intensities has evidenced a large contribution from the orbital moment to the total magnetization. In the antiferromagnetic phase, the orbital moment contributes $17\pm3\%$ to the magnetization density.
[S0163-1829(98)05313-2]

I. INTRODUCTION

Monoxides of $3d$ transition metals, MnO, FeO, CoO, and NiO form an interesting class of materials. Because of their simple crystal and magnetic structures, they have been chosen as test samples for band-theory models. Their insulating behavior contradicts simple electronic band models in which the oxygen p states are fully occupied while the metal s states are empty and the metal d states are partially occupied. To resolve this contradiction, two explanations have been proposed: the Mott-insulator concept[1] and band calculations based on local-spin-density approximation that take into account the antiferromagnetic order.[2] The latter approach implies that orbital moment plays a role in CoO and FeO, while such a contribution is not required in NiO.[3] Furthermore, calculations of magnetic properties of MnO and NiO (Ref. 4) also assumed a vanishing orbital contribution to the anisotropy in the ordered state in contrast with other oxides where the orbital contribution is dominant. On the other hand, measurements of the g factor in diluted paramagnetic NiO (Ref. 5) show deviations from the spin-only value $g=2.0$. Therefore, the determination of the orbital-moment contribution to the magnetization in the ordered state of NiO is a valuable piece of information towards a better understanding of the electronic and magnetic properties of these compounds.

We have undertaken the determination of the orbital-moment magnetization in NiO by means of magnetic x-ray scattering. X-ray methods have proved to be a powerful tool for the study of magnetism. The aspect of interest here is the ability to determine orbital moment in magnetic materials.[6] This separation of spin- and orbital-moment magnetization is possible because in the nonresonant magnetic x-ray scattering cross section, the spin- and the orbital-moment densities have different geometrical prefactors that can be adjusted by changing either the scattering geometry or the x-ray polarization.[7] In the resonant regime, x-ray dichroism or spin-dependent x-ray spectroscopy can also separate orbital and spin contributions with the help of sum rules.[8] Circular and linear dichroism experiments can be applied to ferromagnets and antiferromagnets, but they provide information at zero momentum transfer only. Scattering experiments give access to the momentum transfer dependence and therefore to the spatial extent of spin- and orbital-moment densities. Several magnetic x-ray Bragg scattering experiments[9,10] have been attempted previously in rare-earth and actinides materials to extract the L/S ratio, but the case of $3d$ transition elements or compounds has not yet been considered for two reasons: (1) it is generally assumed that the orbital contribution in these materials is quenched due to the importance of crystal electric fields (CEF) and (2) the magnetic moments are usually small, which leads to weak scattered x-ray signals. Nowadays, third generation synchrotron sources provide highly polarized intense beams which make it possible to detect weak contributions to magnetization densities. Magnetic form factors have been extensively studied by means of polarized neutron diffraction to analyze the spatial extent of the magnetization density. Neutrons do not probe separately spin and orbital moments. However, it is possible to extract these quantities through a modeling of the electronic configuration. In simple rare-earth $(4f)$ and ionic actinide $(5f)$ compounds, the ground state is given by the Russell-Saunders predictions and the orbital and spin moments are rather well known. In transition metal $(3d)$ compounds, the crystalline field interactions are stronger than spin-orbit coupling and the orbital moment is usually reduced. Spins are coupled through pure exchange interactions and the remaining part of the orbital moment is ordered due to spin-orbit coupling. Further effects such as anisotropy and spatial contraction of form factors arise due to the anisotropy of the CEF and to covalency.

Experiments on NiO were performed at several photon energies in the nonresonant regime, below and well above the K edge of nickel (8.33 keV), and in the resonant regime, near the K edge. In this paper, we consider the nonresonant part only because the resonant Bragg scattering does not readily provide information on the orbital moment density. However, recent experiments in transition-metal systems have revealed features in the magnetic-scattering amplitude that are related to solid-state effects.[11] Our results on the resonant scattering in NiO will be presented in a forthcoming paper.

NiO has the NaCl fcc structure with $a=4.177$ Å at room temperature. The ground-state configuration of the Ni^{2+} ion has a $3d^8$ configuration. Below $T_N=523$ K, NiO orders in the type-II antiferromagnetic structure[12] where ferromagnetic planes are stacked antiferromagnetically along the [111] axes with their magnetic moments aligned in the [111] planes along one of the [112] directions.[13] The ordered phase is orthorhombic[14] which gives rise to magnetic domains: four T domains corresponding to the four propagation directions of the antiferromagnetic structure, and within each T domain, three S domains corresponding to the three equivalent orientations of the magnetic moments in the [111] planes. NiO was first chosen by de Bergevin and Brunel[15] as a test sample to demonstrate the feasibility of magnetic x-ray-diffraction experiments using a sealed x-ray tube. Previous synchrotron experiments[16] have shown the existence of resonant effects at the K edge.

The neutron-diffraction determination of the magnetic form factor of NiO by Alperin[17] has revealed that the electron densities are more compact than free atom calculations would predict. Attempts were made to interpret this contraction on the basis of an orbital contribution. The amount of the orbital moment part in the magnetization density was estimated to be 10% based on paramagnetic resonance measurements[5] of g factor that give $g=2.2$. However, including an orbital contribution to the magnetic form factor[18] did not reproduce the wave-vector dependence of the measured magnetic form factor. Attempts to incorporate some covalency effects[19] failed to improve the agreement between the calculated form factor and the observed values. Since the orbital moment plays an important role in the properties of the transition-metal monoxides, we designed this x-ray-scattering study to determine the magnetic form factors, $L(Q)$ and $S(Q)$, as a function of the scattering vector Q in the antiferromagnetic state of NiO.

The presentation of our work is organized as follows. First, we recall briefly the main ingredients of the magnetic x-ray scattering cross section that are of importance to the experiment. We then describe the experimental methods. We have been led to study the magnetic domains distribution, which we comment on. Finally, the results on the magnetic form factors are discussed.

II. SCATTERING CROSS SECTION

The nonresonant magnetic x-ray scattering amplitude has been reviewed by several authors.[6,7] Here, we follow the treatment by Blume and Gibbs.[7] The magnetization-dependent part of the x-ray-scattering amplitude can be written as

$$\langle \mathbf{F}_m \rangle = -r_0 \frac{i\hbar\omega}{mc^2} \langle \mathbf{M}_m \rangle,$$

with

$$\langle \mathbf{M}_m \rangle = \frac{1}{2} \mathbf{L}(\mathbf{Q}) \cdot \mathbf{A} + \mathbf{S}(\mathbf{Q}) \cdot \mathbf{B}, \tag{2.1}$$

where the vectors **A** and **B** contain geometrical factors depending on the scattering geometry and the polarizations of the incident and scattered beams, r_0 is the classical radius of the electron, and $\hbar\omega$ is the incident photon energy. The quantity $\mathbf{S}(\mathbf{Q})$ represents the Fourier transform of the spin-moment density. In general, $\mathbf{L}(\mathbf{Q})$ does not reduce to the Fourier transform of the orbital-moment density; in the case of elastic scattering, it can be associated with a similar expression encountered in the neutron-scattering amplitude[7] which represents an eigenvalue of electronic orbital operators. At $Q=0$, it provides a measure of the orbital-moment magnetization. The polarization dependence of the vectors **A** and **B** allows the distinction of the contributions of L and S to the scattered intensities. The polarization of x rays can be described by two-dimensional vectors. In the case of synchrotron experiments it is natural to choose linear polarization vectors because synchrotron x rays are naturally linearly polarized in the electron orbit plane. In such a vector basis, the scattering amplitude M_m takes the following form:[7]

$$\langle \mathbf{M}_m \rangle = \begin{bmatrix} \langle M_m \rangle_{\sigma\sigma} & \langle M_m \rangle_{\sigma\pi} \\ \langle M_m \rangle_{\pi\sigma} & \langle M_m \rangle_{\pi\pi} \end{bmatrix} = \begin{bmatrix} (\sin 2\theta) S_2 & -2(\sin^2\theta)[(\cos\theta)(L_1+S_1)-(\sin\theta)S_3] \\ 2(\sin^2\theta)[(\cos\theta)(L_1+S_1)+(\sin\theta)S_3] & (\sin 2\theta)[2(\sin^2\theta)L_2+S_2] \end{bmatrix}, \tag{2.2}$$

where 2θ is the scattering angle. The components of $\mathbf{S}(\mathbf{Q})$ and $\mathbf{L}(\mathbf{Q})$ along the three basis vectors defined in Fig. 1 are denoted as S_α and L_α ($\alpha=1,2,3$). The three basis vetors are the same as those defined in Ref. 7. In the case of a general polarization state, the scattered intensities can be calculated in terms of the components given in Eq. (2.2) by using the Poincaré representation for the polarization or the density matrix for the incident beam.[6,7]

III. EXPERIMENTAL CONDITIONS

The experiments presented in this paper were conducted at the ID20 magnetic-scattering beamline at the ESRF. The

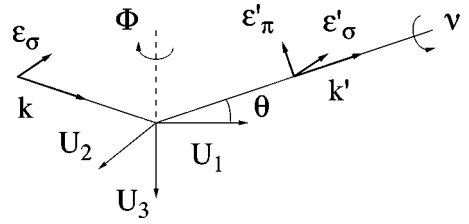

FIG. 1. Scattering geometry and definition of reference axis. **k** and **k**′ are the incident and scattered wave vectors; $\boldsymbol{\epsilon}$ and $\boldsymbol{\epsilon}'$ denote the polarization vectors of the incident and scattered beams. The incident beam is σ polarized. The $\mathbf{U}_1$'s basis vectors are defined as in Ref. 7.

x-ray source is a linear hybrid undulator with a 48 mm period. It delivers photon beam with brilliance around 1.5×10^{19} ph/s/mm^2/mrad^2/0.1% bw around 8 keV at 200 mA. The optics comprise a double Si(111) crystal monochromator and two focusing mirrors on each side of the monochromator.[20] At 7.84 keV using the third harmonics of the undulator, the standard incident power at the sample position is approximately 2.0×10^{12} ph/s at 200 mA with a beam size of 0.3×0.2 mm^2.

The sample was mounted on a diffractometer which allows a four-circle geometry and polarization analysis of the scattered beam. The polarization analyzer crystals that we used are pyrolitic graphite PG(006) and LiF(800) with peak reflectivity of 12 and 10 %, respectively. A sketch of the scattering geometry is given in Fig. 1. Polarization analysis is performed by rotating the analyzer+detector assembly about the scattered beam (rotation angle ν). Denoting the Stokes components of the scattered beam by I_0, P_ζ, P_ξ, and P_η, the intensity $I(\nu)$ collected in the detector as a function the rotation ν of the analyzer crystal is given by[21]

$$I(\nu)\propto\frac{I_0}{2}\,(1+\cos^2 2\theta_p+\cos 2\nu\,\sin^2 2\theta_p P_\zeta + \sin 2\nu\,\sin^2 2\theta_p P_\xi), \tag{3.1}$$

where I_0 is the total power incident on the analyzer crystal and θ_p is the Bragg angle of the analyzer crystal. The origin of ν corresponds to the measure of the horizontal polarization. P_ζ is the linear polarization ($P_\zeta=1$ means that the radiation is fully polarized in the horizontal plane), P_ξ is the polarization at 45°. As expected, the analyzed intensity does not depend explicitly on the circular polarization, P_η. The unpolarized component must be taken into account. Analysis of the incident monochromatic beam leads to $P_\zeta=0.995\pm0.005$, $P_\xi=0.0\pm0.005$ and $P_{\rm unp}$ or $P_\eta<0.01\pm0.01$ over the photon energy range considered here. To a very good approximation, we have taken the square modulus of the components $\langle M_m\rangle_{\sigma\pi}$ and $\langle M_m\rangle_{\sigma\sigma}$ in Eq. (2.2) to be proportional to the scattering cross sections for the rotated and nonrotated intensities, respectively.

Experiments were performed at two different energies 7.84 and 17.4 keV for which the two analyzers crystals, PG(006) and LiF(800), respectively, are perfectly adapted with $\theta_p=90°$. Expression (3.1) assumes that all resolution effects are taken into account by using properly integrated

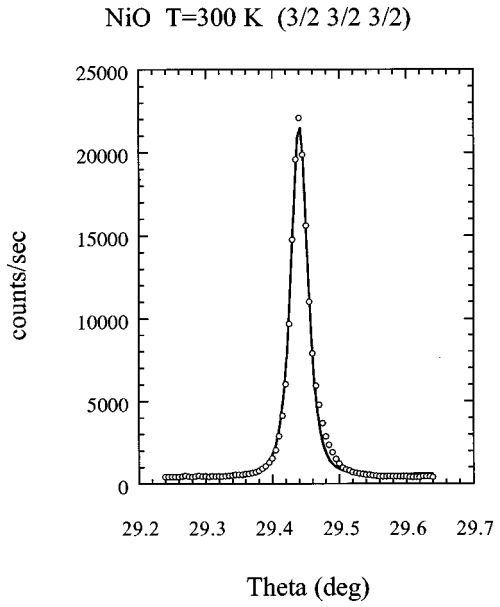

FIG. 2. Rocking curve of the (3/2 3/2 3/2) magnetic reflection at $T=300$ K.

intensities. Indeed, intensities scattered by the sample have been integrated by rocking the sample and the analyzer to take into account the different beam divergences and resolutions in the scattering plane and out of the plane. Proper integration is more readily done with the PG(006) than with LiF(800) because of the broad mosaic spread of PG(006). The narrow mosaic of LiF modifies the instrumental resolution and makes the comparison of integrated intensities rather difficult. Therefore, most the data was taken at 7.84 keV. The nonrotated $I_{\sigma\sigma}$ and the rotated intensity $I_{\sigma\pi}$ were measured at $\nu=0°$ and $\nu=90°$, respectively. We have used standard NaI(Tl) scintillation detectors, planar Si detectors in the photocurrent mode and ion chambers.

IV. EXPERIMENTAL RESULTS

A rocking curve of the magnetic peak (3/2,3/2,3/2) at $T=300$ K is shown in Fig. 2 without polarization analysis. The high count rate in magnetic peaks has encouraged us to make a quantitative use of the scattered intensities even with polarization analysis. In order to extract useful values for the magnetic intensities, we have checked that our experimental procedure gives an adequate description of the crystal structure. For mosaic crystals, integrated specular intensities can be written as[22]

$$I(\mathbf{Q})=I_0\,\frac{\lambda^3 r_0^2}{2\mu v_a^2}\,\frac{|F(\mathbf{Q})|^2}{\sin 2\theta}, \tag{4.1}$$

where μ is the absorption coefficient, v_a is the unit-cell volume, and F^2 is the square of the structure factor expressed in electron units. This applies to ideally imperfect crystals. In the case of crystals of excellent quality like NiO, extinction effects may be important and should be estimated. In the extreme case of an ideally perfect nonabsorbing crystal, Eq. (4.1) should be replaced by[22]

$$I(\mathbf{Q}) = I_0 \frac{8}{3\pi} \frac{\lambda^2 r_0}{v_a} \frac{|F(\mathbf{Q})|}{\sin 2\theta}. \quad (4.2)$$

We have measured the integrated intensities of the (111) and the (222) fundamental reflections of the NiO crystal structure. The incident power has been measured at various energies using a calibrated photodiode. At 7.84 keV, a reflecting power of $(2.7\pm0.2)10^{-4}$ radian has been measured for the (111) Bragg peak and $(9.5\pm0.6)10^{-5}$ radian for the (222) reflection. At 17.41 keV, we have found $(1.35\pm0.1)10^{-4}$ radian and $(7.6\pm0.3)10^{-5}$ radian, respectively. From Eq. (4.1), the values at 7.84 keV translate into a scattering amplitude of 9.8 and 7.2 electrons, respectively, for the two reflections. At 17.4 keV, we obtain 14.2 and 14.8 electrons. The latter result is in remarkable agreement with the calculated values of 15.7 and 16.1 when taking into account the temperature factors[17] $B_{\mathrm{Ni}}=0.37$ and $B_{\mathrm{O}}=0.26$. The reduction of the observed structure factors due to extinction is to be taken into account when comparing magnetic and charge intensities.

As mentioned in the introduction, the magnetic structure of NiO is characterized by a (1/2 1/2 1/2) propagation vector corresponding to one T domain with the magnetic moments aligned in the [111] planes along a [112] direction.[13] When measuring the scattering intensities from a given T domain, all contributions from the associated S domains add incoherently. Therefore, the polarized components of intensities in Eq. (2.2) depend on the relative volume of the S domains and on the relative orientation of the [112] directions with the incident polarization. Since it is impossible to control the domain population at every position of the sample, we have averaged all measured intensities over the domain populations by rotating the sample about the relevant threefold ⟨111⟩ axis. For this purpose, the samples that have been studied are single crystals ($10\times6\times5$ mm^3) of high quality with a [111] face. A [111]-axis normal to the surface was carefully oriented along the Φ axis of the four-circle diffractometer. Specular magnetic reflections (1/2 1/2 1/2), (3/2 3/2 3/2), and (5/2 5/2 5/2) could be measured as a function of the Φ angle at the two different energies. For each reflection, we have measured the total integrated intensities I_{total} measured without polarization analysis, and the polarized components, $I_{\sigma\sigma}$ and $I_{\sigma\pi}$ (Fig. 3).

The magnetic nature of the observed signal is demonstrated by the polarization analysis and the temperature dependence. First, the scattered intensity at the position (3/2 3/2 3/2) vanishes above $T=525$ K a value close to T_N. Second, all observed intensities show a rotated component. In Fig. 3, we have shown the polarization components $I_{\sigma\sigma}$ and $I_{\sigma\pi}$ from the (1/2 1/2 1/2) and (5/2 5/2 5/2) reflections. There exists a large rotated intensity $I_{\sigma\pi}$. Both the spin and the orbital moment rotate the polarization, but only the spin contributes to $I_{\sigma\sigma}$.

A. Magnetic domains

Reflections from domains with propagation vectors different from the surface normal were found to be extremely weak (less than 1%) compared to specular magnetic reflections. The sample appears to be single T domain with propagation vector parallel to the surface normal, at least in the near-surface region probed with 7.84 keV x rays (roughly 40 μm absorption length at both energies).

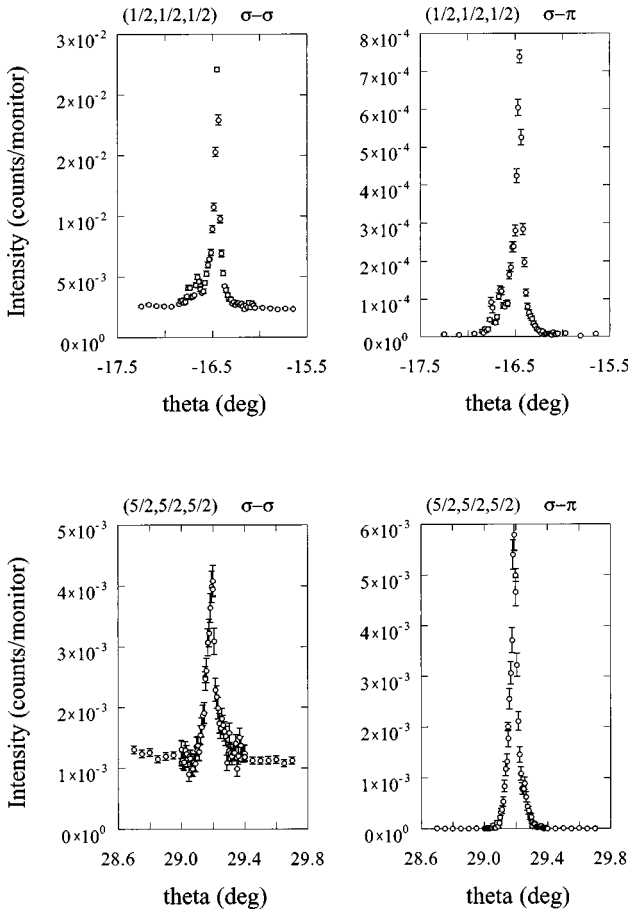

FIG. 3. Polarized components of intensities from the (1/2 1/2 1/2) and (5/2 5/2 5/2) magnetic reflections normalized to monitor counts. The contribution from the orbital moment becomes dominant at large momentum transfer. Background in the σ-π channel is strongly reduced because it originates from charge scattering.

By rotating the sample about the surface normal, we could study the S domain distribution within the [111] T domain. Figure 4 shows the Φ dependence of $I_{\sigma\sigma}$ and $I_{\sigma\pi}$ at the (3/2 3/2 3/2) position. The two intensities exhibit a modulation of period π characteristic of the S-domain distribution. A modulation with a period 2π would indicate that the footprint of the beam is moving across the surface of the sample during the Φ rotation. In a given S domain, the magnetic-scattering amplitudes vary in a simple manner with the Φ angle:

$$M_{\sigma\sigma} = \sin 2\theta \sin \Phi S(\mathbf{Q}),$$

$$M_{\pi\sigma} = \sin 2\theta \sin \theta(\cos \Phi S(\mathbf{Q}) + \cos(\Phi+\Phi_0)L(\mathbf{Q})), \quad (4.3)$$

where an angular Φ_0 offset is allowed between S and L. The origin of Φ is taken with the spin direction in the scattering plane. In a multi-S-domain sample, scattered intensities are combinations of $\sin^2\Phi$ and $\cos^2\Phi$.

The two polarized components are exactly $\pi/2$ shifted in Φ, which is in agreement with a collinear arrangement for

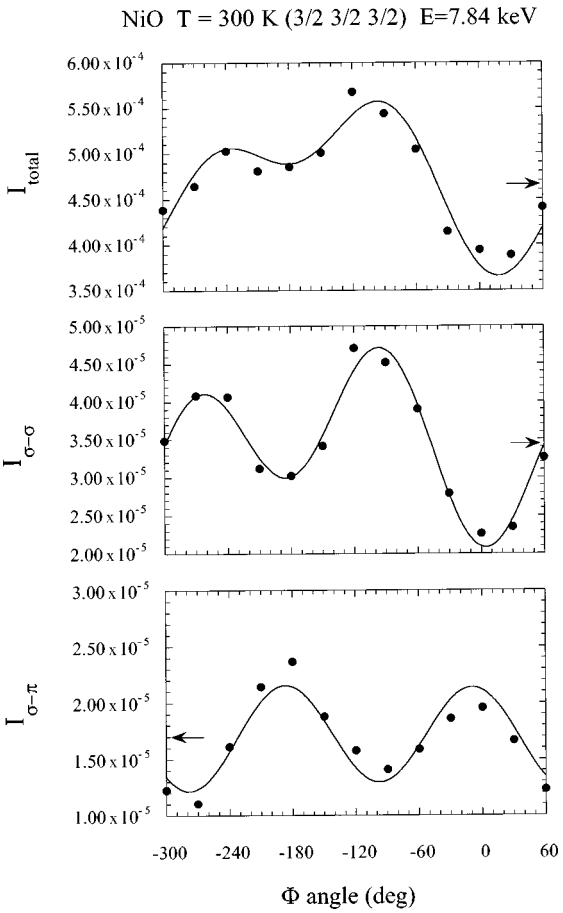

FIG. 4. Normalized integrated intensities of the (3/2 3/2 3/2) reflection as a function of Renninger angle Φ at 7.84 keV. Intensities are given in (radians*detector counts/monitor counts). Errors bars are smaller than the dot size. The two polarized components, $I_{\sigma\sigma}$ and $I_{\sigma\pi}$, are out of phase by $\pi/2$. The total intensity is the sum of the two components corrected for the reflectivity of the PG(006) analyzer. Arrows indicate the Φ averaged values that are used to extract $L(\mathbf{Q})$ and $S(\mathbf{Q})$. The full lines show calculated superposition of periods π and 2π (see text).

the spin and orbital moment, $\Phi_0=0$. The Φ dependence can be used to determine the fractional volumes of the three S domains $\alpha_{i=1,2,3}$ probed by the incident x-ray beam; in the case of Fig. 4, we deduce $\alpha_1=0.26\pm0.03$, $\alpha_2=0.23\pm0.03$, and $\alpha_3=0.50\pm0.02$.

To better characterize the S domains, we have translated the sample by amounts comparable to the beam footprint size, i.e., 300 μm. The shape of the Φ dependence changes drastically through such translations, indicating that S domains in our samples have lateral dimensions of less than 300 μm. Such dimensions ensure us that a proper averaging can be made by rotating Φ. Neutron topography experiments[13] have revealed similar dimensions for S domains in thin NiO crystals, but with large shape anisotropy.

B. Magnetic form factors

Polarized components shown in Fig. 4 have been corrected for changes in the width of the rocking curve of analyzer crystals at various ν angles in order to fully integrate scattered intensities. The normalization of $I_{\sigma\sigma}+I_{\sigma\pi}$ to I_{tot} provides an independent determination of the reflectivity of the crystal analyzer. The peak reflectivity of the PG(006) analyzer at 7.84 keV is found to be (12.5 ± 0.5) %. From the Φ dependence of the magnetic intensities, we have extracted averaged values for the integrated magnetic intensities as shown in Table I. These averaged intensities correspond to $\langle\sin^2\Phi\rangle=\langle\cos^2\Phi\rangle=1/2$ in the magnetic-scattering cross section after the squaring of Eq. (4.3), and allow a straightforward determination of the ratio $L(Q)/2S(Q)$ (Fig. 5). The results in Fig. 5 clearly show that a large contribution (17 ±3%) to the magnetization from the orbital moment exists in NiO. The increase of $L(Q)/2S(Q)$ with the scattering vector reflects the broader spatial extent of the spin density. The orbital contribution enhances the spin-alone magnetic moment to make the total moment eventually larger than $2\mu_B$ as expected for spin-only magnetic moment ($S=1$).

TABLE I. Φ-averaged intensities normalized to monitor counts at 7.84 keV. Intensities are expressed in (radians* detector counts/monitor counts). The data can be used to extract the $L(\mathbf{Q})/2S(\mathbf{Q})$ ratio.

(h,k,l)	$I_{\sigma\sigma}$	$I_{\sigma\pi}$	I_{total}
$\left(\frac{1}{2}\frac{1}{2}\frac{1}{2}\right)$	$(2.8\pm0.1)10^{-5}$	$(1.32\pm0.08)10^{-6}$	$(2.35\pm0.2)10^{-4}$
$\left(\frac{3}{2}\frac{3}{2}\frac{3}{2}\right)$	$(3.45\pm0.1)10^{-5}$	$(1.7\pm0.05)10^{-5}$	$(4.5\pm0.3)10^{-4}$
$\left(\frac{5}{2}\frac{5}{2}\frac{5}{2}\right)$	$(3.5\pm0.1)10^{-6}$	$(6.2\pm0.2)10^{-6}$	$(7.7\pm0.4)10^{-5}$

Comparison of the magnetic intensities to the charge peaks and extinction corrections have been made to put magnetic structure factors on an absolute scale as in Eq. (4.1).

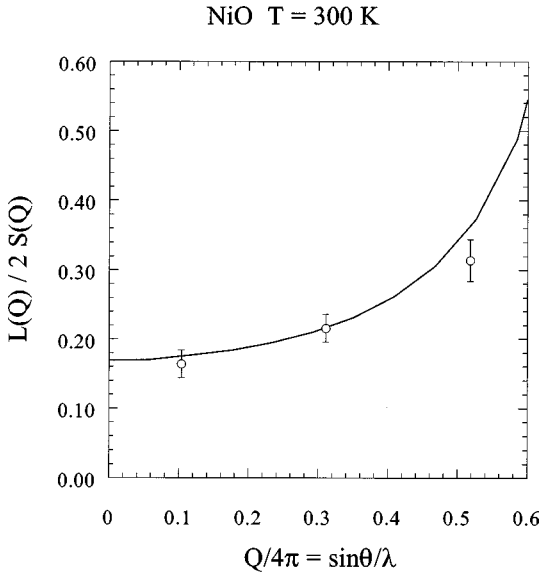

FIG. 5. Measured variation of $L(\mathbf{Q})/2S(\mathbf{Q})$ as a function of $\sin\theta/\lambda=\mathbf{Q}/4\pi$. The continuous line is the K dependence estimated by Blume (Ref. 18) adjusted to fit through the data with a contraction of the wave function by 17%. $L(\mathbf{Q})/2S(\mathbf{Q})$ extrapolates to 0.17 at $\mathbf{Q}=0$.

TABLE II. Φ-averaged structure factors squared expressed in electron units per Ni atom and corrected for the Debye-Waller factor of Ni. These results have been obtained after a normalization to the (111) and (222) charge peak intensities at 7.84 keV. The error bars reflect the normalization uncertainties. The scale factor used here is $(1.1\pm0.1)\times10^{-3}$. Polarized intensities have been corrected for the analyzer reflectivity (see text).

(h,k,l)	$F^2_{\sigma\sigma}$	$F^2_{\sigma\pi}$	F^2_{total}
$\left(\frac{1}{2}\frac{1}{2}\frac{1}{2}\right)$	$(8.4\pm0.9)10^{-6}$	$(4.0\pm0.5)10^{-7}$	$(9\pm1)10^{-6}$
$\left(\frac{3}{2}\frac{3}{2}\frac{3}{2}\right)$	$(3.2\pm0.4)10^{-5}$	$(1.6\pm0.2)10^{-5}$	$(4.8\pm0.5)10^{-5}$
$\left(\frac{5}{2}\frac{5}{2}\frac{5}{2}\right)$	$(4.2\pm0.5)10^{-6}$	$(7.5\pm0.9)10^{-6}$	$(1.1\pm0.2)10^{-5}$

Resulting values for the magnetic structure factors are given in Table II. Extinction effects were corrected as mentioned above and we have included the Debye-Waller factor correction for Ni atoms. As observed experimentally, we have further assumed that the region of the crystal probed by the 7.84 keV x rays was a single T domain. Experimental uncertainties are dominated by the normalization to the charge peaks. By using the scattering amplitude Eq. (4.3) and the prefactor in Eq. (2.1), we have extracted the spin- and orbital-moment form factor in absolute numbers. The resulting values are shown in Fig. 6 as a function of the scattering vector. The extrapolated values at zero scattering vector, $S(0)=0.95\pm0.1$ and $L(0)=0.32\pm0.05$, lead to a value of $2.2\pm0.2\mu_B$ for the staggered magnetization at $T=300$ K. This is in close agreement with neutron results giving $1.81\pm0.2\mu_B$ (Ref. 17) and $1.97\mu_B$.[23]

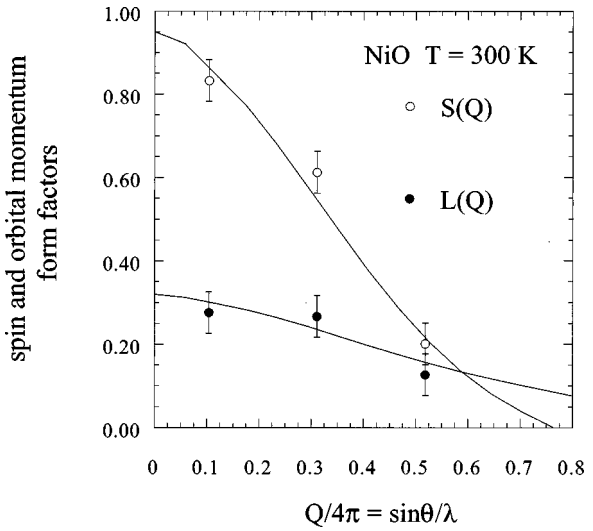

FIG. 6. Spin form factor and orbital-moment form factor in NiO. The data have been obtained by normalizing magnetic intensities to charge peaks corrected for extinction. Extrapolations at $K=0$ provide a value for the thermal average of $S=0.95\pm0.10$ and $L=0.32\pm0.05$ which lead to a value of $2.2\pm0.3\mu_B$ for the staggered magnetization at $T=300$ K. The continuous lines are the calculated variations of $S(\mathbf{Q})$ and $L(\mathbf{Q})$ with $\sin\theta/\lambda$ from Refs. 18 and 24 with an expansion of the $\mathbf{Q}$ scale by 17%.

V. DISCUSSION

In Fig. 6, the continuous lines represent the scattering vector dependence of the spin- and the orbital-moment form factors as calculated by Watson[24] and Blume.[18] The values at $Q=0$ have been adjusted to fit the data. Furthermore, our results indicate also a contraction of the atomic wave functions for Ni in NiO. Following Alperin,[17] we have expanded the scattering vector by 17% to obtain a fair agreement through the only three experimental values. Even if more experiments are needed to clarify this point, our present results indicate a contraction of the electronic wave functions similar to that observed with neutrons. Furthermore, we observe that the thermal average spin moment at 300 K is close the saturated value. It should be noted that covalency effects in NiO (Ref. 23) have have been shown to be of the order of 3%.

Returning to the L/S determination, we have confirmed that the residual orbital moment is parallel to the spin, as expected from simple spin-orbit coupling for a $3d^8$ free atom. The extrapolation at $Q=0$ shows that the effective L/S ratio amounts to $L/S=0.34$. This large contribution is surprising in transition-metal oxides like NiO where L is supposed to be largely quenched. It would be appropriate to take into account this large residual orbital moment when discussing the electronic and magnetic properties of NiO.

We have observed that the near-surface region in our NiO sample was almost single T domain, as observed also by Hill *et al.*[16] We note that this single-domain structure of the near-surface region is not a general feature of antiferromagnetic materials. Similar behavior has been found in pure Cr sample[25] but we have examples[26] where different T domains coexist near the sample surface.

These experiments represent an attempt to extract the orbital contribution to the magnetization in NiO with magnetic x-ray scattering. We have shown that the magnetization densities in a simple system like NiO is not yet fully understood. More experiments are needed to unravel the exact origin of the orbital contribution in transition-metal monoxides. Studies on MnO and CoO are in progress to compare two extreme conditions, zero orbital moment and large orbital moment contribution to magnetism, to the intermediate case of NiO. A point of interest would be to test the contribution from the ligands to the magnetic form factors. Such a contribution would appear at very low scattering vector[19] where no Bragg peak is available in crystals. One method to access this range of scattering vector would be to perform x-ray dichroism experiments on a saturated paramagnetic system where magnetic reflectivity could be measured with circular polarization.

ACKNOWLEDGMENTS

We thank A. Stunault and D. Wermeille for their help in analyzing the data, and G. H. Lander and N. Bernhoeft for critical comments on the manuscript. Fruitful discussions with M. Blume are also acknowledged. C.G. wishes to thank the ESRF staff for their hospitality during this work.

[1] N. F. Mott, Proc. Phys. Soc. London, Sect. A **62**, 416 (1949); B. H. Brandow, Adv. Phys. **26**, 651 (1977).
[2] K. Terakura, A. R. Williams, T. Oguchi, and J. Kübler, Phys. Rev. Lett. **52**, 1830 (1984).
[3] K. Terakura, T. Oguchi, A. R. Williams, and J. Kübler, Phys. Rev. B **30**, 4734 (1984).
[4] J. Kanamori, Prog. Theor. Phys. **17**, 177 (1957).
[5] W. Low, Phys. Rev. **109**, 247 (1958).
[6] F. de Bergevin and M. Brunel, Acta Crystallogr., Sect. A: Cryst. Phys., Diffr., Theor. Gen. Crystallogr. **37**, 324 (1981); M. Blume, J. Appl. Phys. **57**, 3615 (1981).
[7] M. Blume and D. Gibbs, Phys. Rev. B **37**, 1779 (1988).
[8] B. T. Thole, P. Carra, F. Sette, and G. van der Laan, Phys. Rev. Lett. **68**, 1943 (1992); P. Carra, B. T. Thole, M. Altarelli, and X. Wang, *ibid.* **70**, 694 (1993).
[9] D. Gibbs, D. R. Harshmann, E. D. Isaacs, D. B. McWhan, D. Mills, and C. Vettier, Phys. Rev. Lett. **61**, 1241 (1988).
[10] D. B. McWhan, C. Vettier, E. D. Isaacs, G. E. Ice, D. P. Siddons, J. B. Hastings, C. Peters, and O. Vogt, Phys. Rev. B **42**, 6007 (1990); S. Langridge, G. H. Lander, N. Bernhoeft, A. Stunault, C. Vettier, G. Grübel, C. Sutter, F. de Bergevin, W. J. Nuttal, W. G. Stirling, K. Mattenberger, and O. Vogt, *ibid.* **55**, 6392 (1997).
[11] A. Stunault, C. Vettier, F. de Bergevin, D. Wermeille, N. Bernhoeft, Th. Brückel, and J. Y. Henry (unpublished).
[12] C. G. Shull, W. A. Strauser, and E. O. Wollan, Phys. Rev. **83**, 333 (1951).
[13] J. Baruchel, M. Schlenker, K. Kurusowa, and S. Saito, Philos. Mag. B **43**, 853 (1981).
[14] W. L. Roth, J. Appl. Phys. **31**, 2000 (1960).
[15] F. de Bergevin and M. Brunel, Phys. Lett. **39A**, 141 (1972).
[16] J. P. Hill, C.-C. Kao, and D. F. McMorrow, Phys. Rev. B **55**, R8662 (1997).
[17] H. A. Alperin, J. Phys. Soc. Jpn. **17**, 12 (1962); Phys. Rev. Lett. **6**, 55 (1961).
[18] M. Blume, Phys. Rev. **124**, 96 (1961).
[19] W. Marshall and S. W. Lovesey, *Theory of Thermal Neutron Scattering* (Oxford University Press, Oxford, 1971), p. 222.
[20] A. Stunault, C. Vettier, F. de Bergevin, N. Bernhoeft, V. Fernandez, S. Langridge, E. Lidström, J. E. Lorenzo-Diaz, D. Wermeille, L. Chabert, and R. Chagnon, J. Synchrotron Radiat. (to be published).
[21] F. Vaillant, Acta Crystallogr., Sect. A: Cryst. Phys., Diffr., Theor. Gen. Crystallogr. **33**, 967 (1977) [in French].
[22] B. E. Warren, *X-ray Diffraction* (Dover, New York, 1990), p. 326.
[23] B. E. Fender, A. J. Jacobson, and F. A. Wegdewood, J. Chem. Phys. **48**, 990 (1968).
[24] R. E. Watson and A. J. Freeman, Acta Crystallogr. **14**, 27 (1961).
[25] J. P. Hill, G. Helgesen, and D. Gibbs, Phys. Rev. B **51**, 10 336 (1995); P. C. de Camargo, A. J. A. de Oliveira, C. Giles, and C. Vettier (unpublished).
[26] A. Stunault, S. Langridge, C. Vettier, D. Gibbs, and N. Bernhoeft, Phys. Rev. B **55**, 423 (1997); N. Bernhoeft, A. Stunault, C. Vettier, F. de Bergevin, D. Gibbs, T. R. Thurston, S. M. Shapiro, J. B. Hastings, P. Dalmas, G. Helgesen, and O. Vogt, J. Magn. Magn. Mater. **140-144**, 1421 (1995).